Detailed Measurements of the Flow Field in a Transonic Turbine Cascade

E. DETEMPLE-LAAKE
DLR, Institute for Experimental Fluid Mechanics
Bunsenstr. 10, D-3400 Göttingen, FRG

ABSTRACT

Systematic experimental investigations of the transonic flow through a plane cascade consisting of profiles designed for a highly loaded gas turbine rotor of a high pressure stage were performed. The experiments comprise side wall pressure distribution measurements in a blade passage and both profile pressure distribution and wake traverse measurements in various planes from midspan to the side wall. The parameters varied are the inlet flow angle and the downstream Mach number. Schlieren photographs and oil flow patterns on the blades and on the side wall are included. The experimental results are interpreted with respect to the existing flow models describing shock wave boundary layer interactions and secondary flow effects. The experimental data are compared with three-dimensional viscous numerical results.

NOMENCLATURE

c^*	throat width
l	blade chord
l_x	axial chord
Ma_2	downstream Mach number
Ma_{Kon}	isentropic profile contour Mach number
p_{01}	inlet flow total pressure
p_{02}	outlet flow total pressure
Re	Reynolds number (based on bitangential chord)
t	blade pitch
x_{Bi}	bitangential coordinate
β_1	inlet flow angle
β_2	downstream flow angle
β_S	stagger angle
ζ	total pressure loss ($\zeta = 1 - p_{02}/p_{01}$)

INTRODUCTION

High turning and high transonic exit Mach numbers resulting in complex transonic flow fields reduce the turbine efficiency level. As the special case may be an individual constellation of profile losses, secondary flow losses, tip clearance losses, shock losses, trailing edge losses results. In dependence on the turning the secondary flows generated by the side wall boundary layers may be large and hence influence significantly the generation of losses. In turbines the side wall secondary losses may amount to half of the total losses ([1] - [3]). The secondary flows also cause a deviation of the exit flow angle. For this reason three-dimensional flow phenomena and losses in the side wall regions of turbine blades are of essential interest for the design of turbine blades. Secondary flows in plane cascades were investigated over a wide range of various parameters such as Mach number, incidence, inlet boundary layer, high inlet turbulence, Reynolds number, aspect ratio, inlet skew (for example compare [4] - [10]).

In the present paper experimental investigations of the three-dimensional flow field in a transonic turbine cascade comprising shock wave boundary layer interaction and secondary flow phenomena are presented. The experiments were carried out with a plane cascade of profiles designed by MTU for a highly loaded gas turbine rotor of a high pressure stage. A sequence of joint investigations was performed by the DLR Institute for Experimental Fluid Mechanics, Göttingen and MTU, München. The measurement techniques used comprise: surface pressure measurements, trailing edge wake traverse measurements, schlieren visualization ([11]), infrared image technique, surface oil flow visualization ([12]), heated thin film measurements ([13]). Thereby a cascade is given which is well known in detail.

On this basis the main objective of the present investigations is to extend the existing knowledge of the flow field at midspan to the flow phenomena resulting from side wall effects and three-dimensional separation. The experimental results are interpreted with respect to the existing flow models describing secondary flow effects ([14] - [16]) and shock wave boundary layer interactions ([17], [18]). The

results of the various experimental investigations are consistent with each other. They are in good agreement with the underlying flow models. Additionally the experimental data provide a test case for the validation of accompanying 3D viscous numerical simulations ([19], [20]). The future investigation planned is the spatial resolution of the secondary flow phenomena by the method of laser light sheet.

The following experimental investigations were performed: side wall pressure distributions, profile pressure distributions along the span, total pressure loss and downstream flow angle along the span. The test programme comprised the variation of the downstream Mach number Ma_2 in the range $0.7 \leq Ma_2 \leq 1.3$ at four different inlet flow angles $\beta_1 = 120°, 140°, 150°, 155°$ (the cascade was designed for $\beta_1 = 130°$). The test Reynolds numbers vary as a function of the Mach number in the range 0.73 to 0.94 $\cdot 10^6$.

EXPERIMENTAL METHODS

The experiments were carried out in the plane cascade wind tunnel of the DLR Göttingen (Fig. 1). The test facility is described in [21]. The wind tunnel is a suction type tunnel with an open circuit which operates intermittently or continuously. Figure 2 shows a typical arrangement of the test section. Due to the test section geometry the blade span is 125 mm. The blade chord length is 60 mm. The test section height is variable between 200 and 380 mm. The test section can accomodate 8-12 blades of high deflection geometry and about 20 blades of low deflection geometry. The cascade geometry based on bitangential coordinates is shown in Figure 3.

The optical setup for schlieren visualization is arranged conventionally. The photographs were taken using a flash light of 50 nanoseconds duration. The surface oil flow pictures were taken by coating the blade and side wall surfaces with a mixture of titanium dioxide powder and baby oil. The side wall pressures were measured in one passage by use of an exchangable side wall with 196 pressure tappings of 0.4 mm diameter in a 5 x 5 mm grid. The test area covered by the pressure tappings is shown in Figure 3 right. For profile pressure measurements one of the blades is replaced by an instrumented blade of 290 mm blade span in order to allow a movement of the plane with the pressure tappings across the whole test section. For data acquisition see [21]. The characteristical cascade flow quantities are determined by local pressure measurements in the wake using a wedge type probe ([22]). These inhomogeneous data are transformed to the homogeneous outlet flow quantities total pressure loss and downstream flow angle by applying the method described in [23].
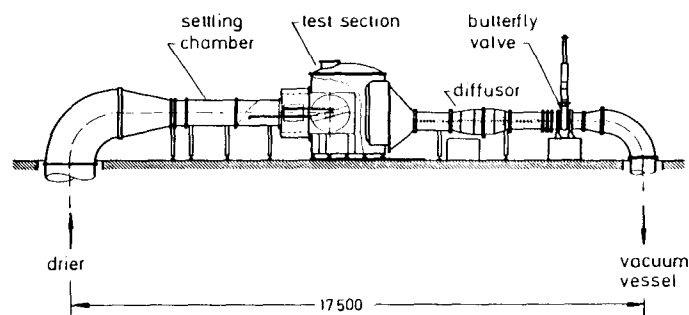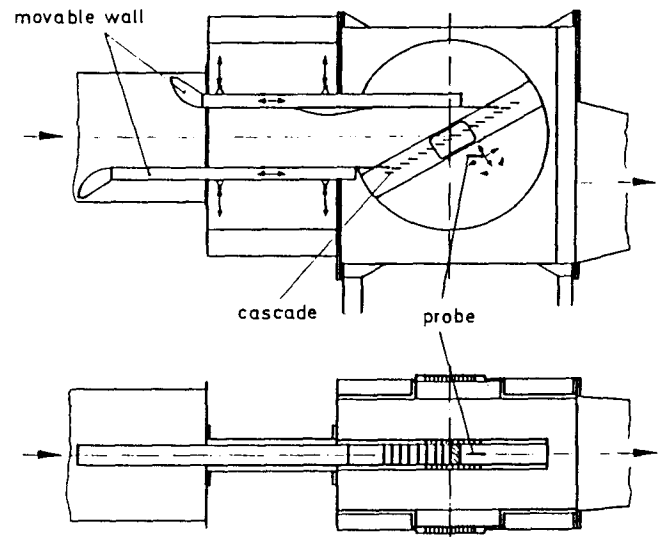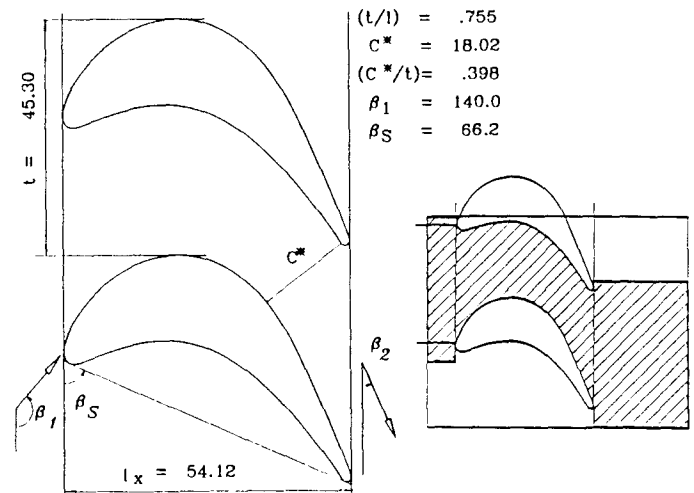

Fig. 1: Wind tunnel

Fig. 2: Test section

Fig. 3: Cascade geometry and test area

EXPERIMENTAL RESULTS

The general features of the midspan flow field with increasing downstream Mach number are illustrated in Figure 4. In the subsonic case, $Ma_2 = 0.9$, the flow is strongly accelerated along the suction side. The expansion of the flow down to the throat results in local supersonic regions indicated by the compression fans. They are limited by the sonic line in the passage and are terminated downstream by a normal shock. At the trailing edge on the pressure side a Prandtl-Meyer-expansion occurs. The wake consists of the pressure and suction side boundary layers which form a Kármán vortex street. At $Ma_2 = 1.0$ the cascade is choked. The acceleration of the flow to high local Mach numbers results in a strong normal shock. The upstream travelling sound waves generated by the vortex separation now accumulate in the trailing edge shocks. With further increase of the downstream Mach number the trailing edge shocks become stronger and more oblique. The typical transonic
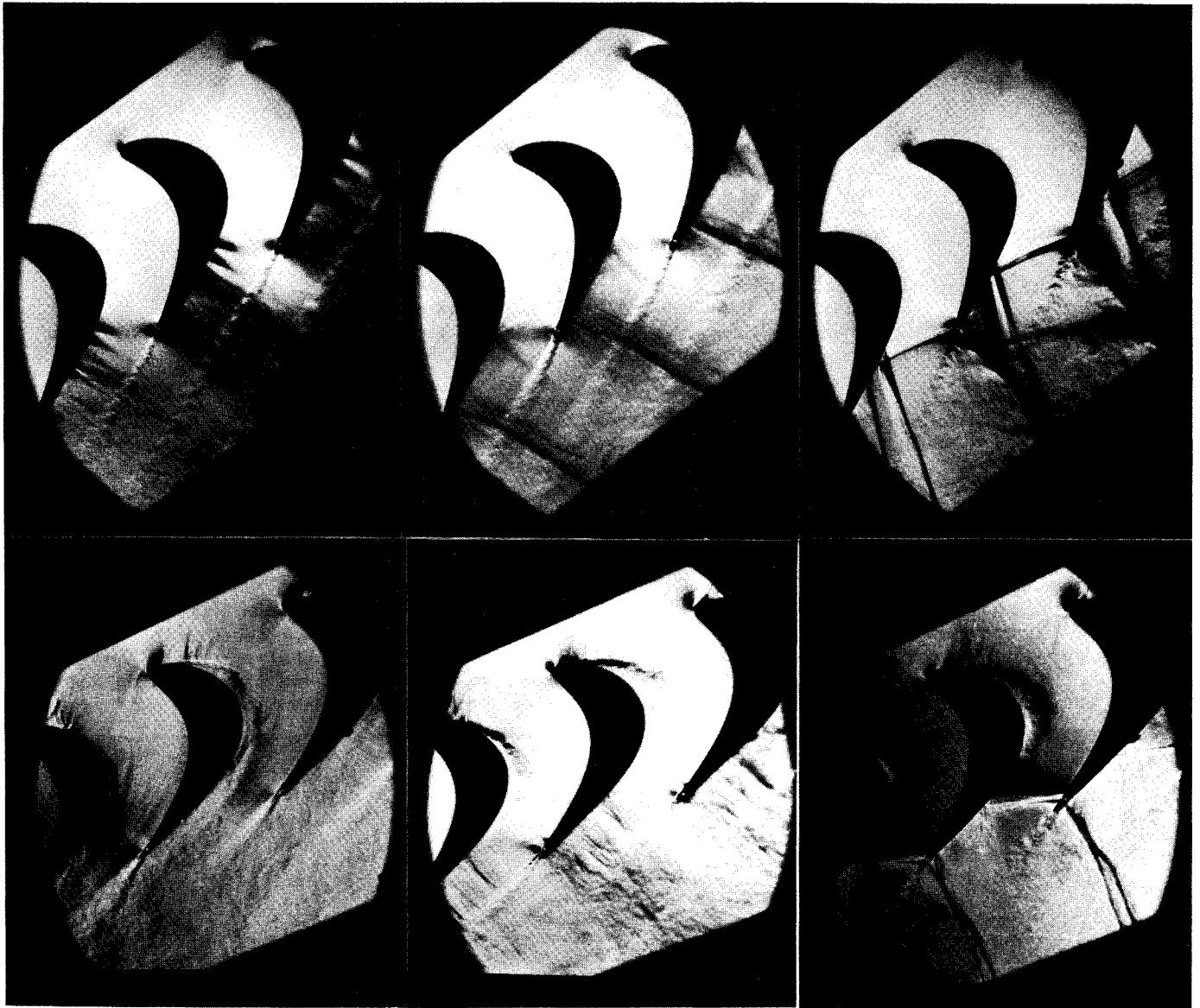
- 2 -

Fig. 4: Schlieren pictures $\beta_1 = 140°$ (top), $\beta_1 = 155°$ (bottom); subsonic case (left), sonic case (mid), super-sonic case (right)

flow pattern at $Ma_2 = 1.25$ comprises a system of trailing edge shocks, deflected shocks and reflected shocks. The suction side trailing edge shock is deflected by the upper wake. The pressure side trailing edge shock is reflected at the lower suction side as a sequence of compression - expansion - compression waves due to the wedge shaped thickened boundary layer. As the result of the pressure gradient related to the impingement of the upper trailing edge shock the laminar boundary layer has lifted and a separation bubble has developed. The heated thin film measurements ([13]) have revealed that the separated boundary layer is turbulent after reattachment. It is not yet clear where the transition from laminar to turbulent occurs.

The flow structures develop qualitatively analoguous for $\beta_1 = 120°$, 140°, 150°. However, at $\beta_1 = 155°$ (Fig. 4 bottom) the flow separates for all Mach numbers at the suction surface downstream of the leading edge leading to a shock. Schlieren pictures and oil flow patterns in connexion with

surface pressure measurements and heated thin film measurements ([12], [13]) reveal a separation bubble at the blade nose. The flow reattaches turbulent shortly behind the separation. At $Ma_2 = 1.25$ the pressure side trailing edge shock impinges on the lower suction side. The fully turbulent boundary layer resists the pressure rise due to the impingement of the shock; no separation bubble occurs. There is no indication of a relaminarisation of the boundary layer.

The associated flow structures on the side wall and on the blade suction surface for a subsonic and a supersonic case are shown in Figures 5 and 6. Figure 5 left shows the subsonic case. The rolling up of the side wall boundary layer in front of a blade into the leading edge horseshoe vortex causes the separation saddle point (S), i.e. distinct flow regions are delimited by the 3D separation lines and the stagnation streamline. Along the stagnation streamline (1) the inlet boundary layer divides into the fluid entering the suction leg of the horseshoe vortex and the fluid forming the
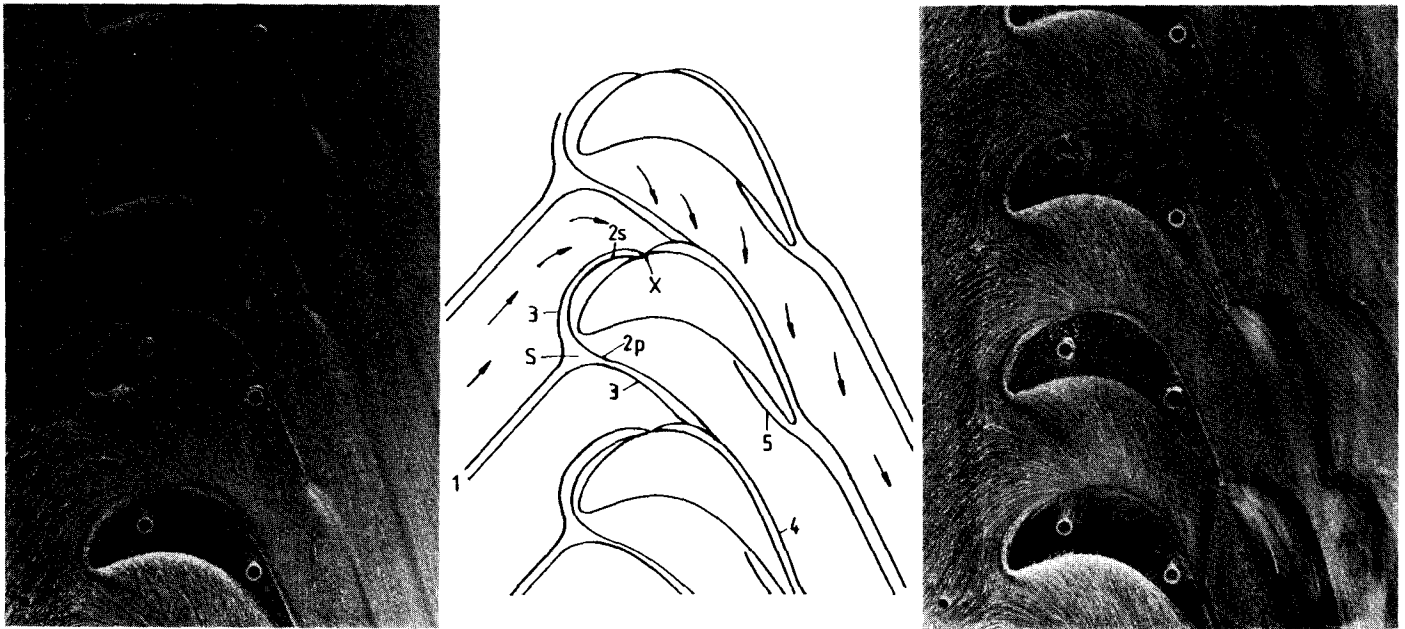
- 3 -

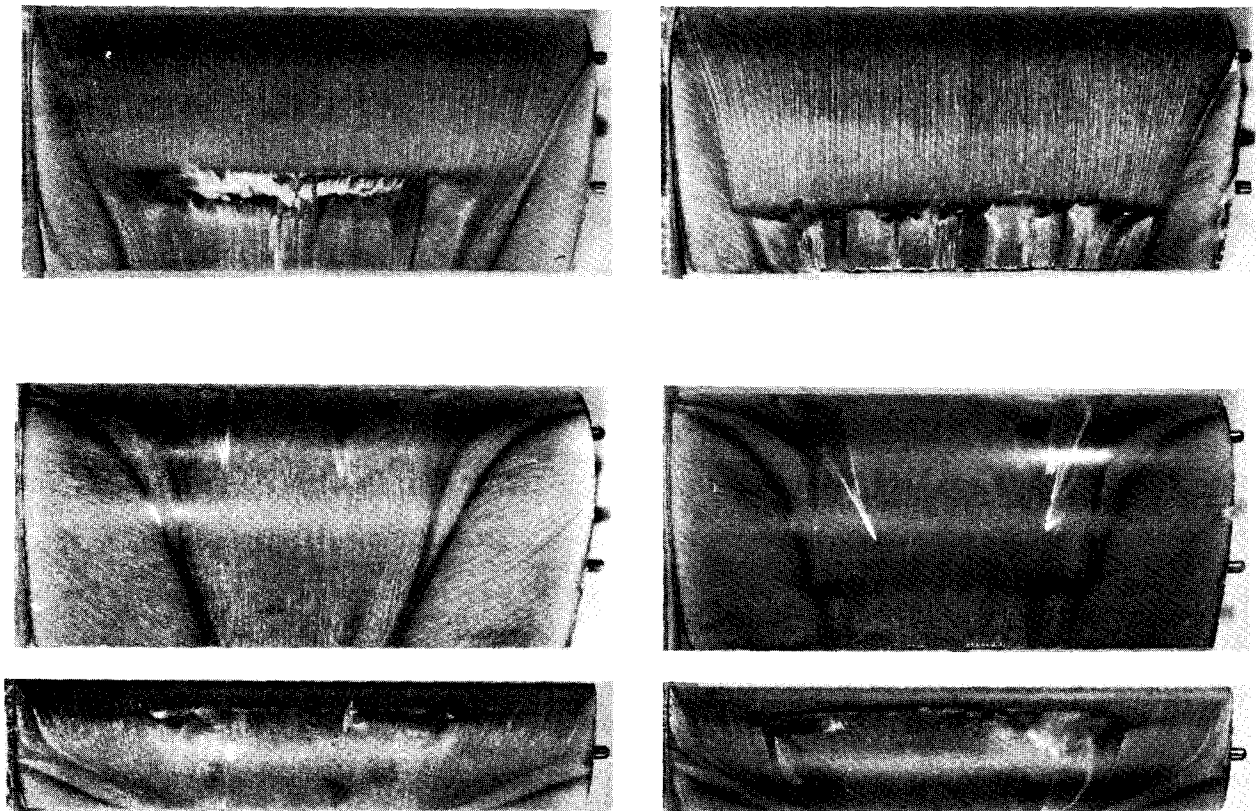Fig. 5: Surface oil flow patterns on the side wall: subsonic case (left), supersonic case (right)

Fig. 6: Surface oil flow patterns on the suction surface: $\beta_1 = 140°$(top), $\beta_1 = 155°$ (bottom); subsonic case (left), supersonic case (right)

- 4 -

pressure leg which merges with the passage vortex in the passage. The two major separation lines ahead of the leading edge are the liftoff line of the horseshoe vortex (2) and the boundary layer separation line (3) ahead of the horseshoe vortex. They merge while swinging around the leading edge. The suction leg of the horseshoe vortex is swept onto the suction surface behind the leading edge due to the transverse pressure gradient in the blade passage. The associated separation line (2s) interferes with the suction side: the vortex leg moves on the blade suction side towards the midspan and touches the separation bubble (Fig.6 top left). The separation line is visible up to the trailing edge. The pressure leg of the horseshoe vortex is deflected towards the suction side of the adjacent blade due to the transverse pressure gradient. On its way the pressure leg merges with the existing passage vortex to one single vortex. In the suction surface flow pattern the side wall side separation line denotes the separation of the passage vortex from the suction surface. On the side wall side of the separation line of the passage vortex - in the corner of suction side and side wall - the separation of the suction side end wall corner vortex is revealed. The side wall flow pattern shows the associated separation line (4) originating downstream of the intersection point (X) of the suction leg with the suction surface. Also a pressure side endwall corner vortex is indicated by a reattachment line (5) on the side wall along the corner of pressure side and side wall. For the supersonic case in principle the oil flow patterns show qualitatively the same features. Additionally, the trailing edge shock traces are revealed which coincide with the shock locations in the midspan known from schlieren pictures and thin film measure-

ments. The skin friction lines are strongly deflected in the shock foot regions. They turn parallel to the shock direction and then continue downstream of the shock in outlet flow direction. The lines' crossing of the shock traces indicates an interaction without separation.

The surface oil flow patterns of $\beta_1 = 140°$ (Fig. 6 top) clearly reveal a separation bubble on the suction surface also in the subsonic case which is not visible in the schlieren pictures but is revealed by heated thin film measurements ([13]) and profile pressure measurements (Fig. 8). The oil flow patterns at $\beta_1 = 155°$ (Fig. 6 bottom) show a separation bubble at the blade nose and a larger extension of the passage vortex towards the midspan. At $Ma_2 = 1.25$ the separation lines of the suction leg of the horseshoe vortex and the passage vortex are deflected by the impinging shock. No separation bubble due to the shock impingement is observed.

Figure 7 shows the isobars on the side wall resulting from the side wall pressure measurements for $\beta_1 = 140°$ and $\beta_1 = 155°$. In contrast to the three-dimensional presentation of the results ([24]) which additonally reveals the local pressure extremes the isobars do not resolve local phenomena. In the case of $\beta_1 = 140°$ the isobars in coincidence with the wall streamlines show a strong negative pressure gradient across the blade passage. Along the separation line of the passage vortex across the blade passage kinks of the isobars are visible. The wall streamlines show the imprints of the legs of the horseshoe vortex and the passage vortex. In the sonic and supersonic case (Fig. 5) the suction side trailing edge shock leaves its imprint on the side wall. The shock wave boundary layer interaction does not extend to
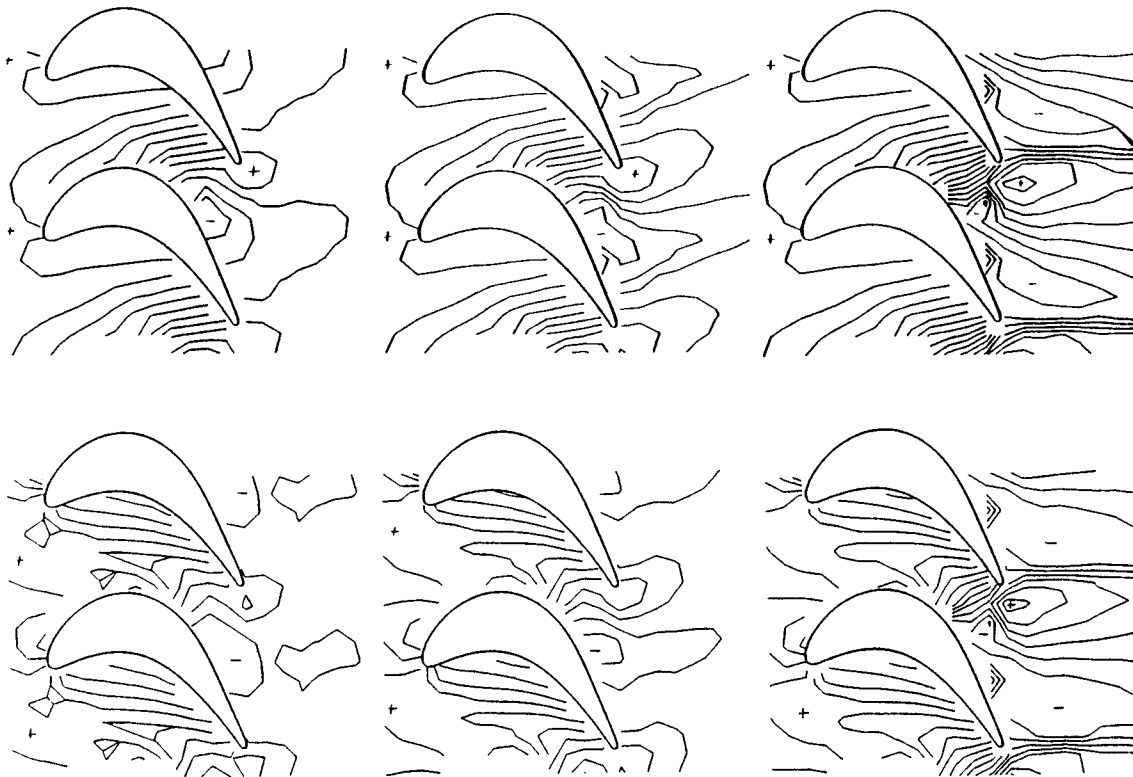
Fig. 7: Side wall pressure distributions; $\beta_1 = 140°$ (top), $\beta_1 = 155°$ (bottom); subsonic case (left), sonic case (mid), supersonic case (right)

- 5 -

the side wall and hence the separation bubble does not leave any foot print on the side wall.

The isobars show the static pressure imprints of the reflected trailing edge shock indicated by the pressure minimum on the suction surface. With increasing Mach number this pressure minimum moves downstream in coincidence with the locations of the separation bubbles in the suction side surface oil flow pictures (Fig. 6 top). The stagnation point at the blade nose and the intersection point on the suction surface are indicated by diverging isobars. The pressure maximum (+) in front of the blade nose is related to the flow separation.

The isobars for $\beta_1 = 155°$ (Fig. 7 bottom) show the upstream movement of the stagnation point and the intersection point along the suction side due to the positive incidence. This tendency coincides with the oil flow patterns (Fig. 6 bottom). In this case the saddle point in front of the blade nose also is resolved in the test area by a pressure maximum. The distortion of the isobars due to the flow separation behind the blade nose is clearly visible.

Profile Mach number distributions were measured along the span (Fig. 8) in order to link the side wall and suction surface flow patterns. As representative cases four

different sections, 50% (midspan), 14%, 8%, 1.6% (side wall), for a subsonic, sonic and supersonic case are shown. The profile Mach number distributions easily can be interpreted in connexion with the schlieren pictures (Fig. 4 top). In the subsonic case, $Ma_2 = 0.9$, at midspan (Fig. 8 top left) the Mach number distribution reveals the strong acceleration of the flow along the suction surface. At 57 % bitangential chord length the laminar boundary layer separates and a separation bubble exists. The normal shock at 76 % chord length which terminates the local supersonic regions known from the schlieren pictures decelerates the flow to subsonic velocities. In the spanwise region from 14.4 % blade height to the side wall no more separation bubbles and normal shocks are revealed in accordance with the oil flow pictures. The velocities decrease towards the wall. This region is dominated by the passage vortex. The pressure side Mach number distributions along the blade span are qualitatively similar, only the velocities increase towards the side wall region. In the supersonic case, $Ma_2 = 1.25$, the Mach number distribution along the suction side is characterized by the shock wave boundary layer interaction due to the impinging shock from the upper blade. The resulting separation bubble which extends from 70 % to 80 % bitan-
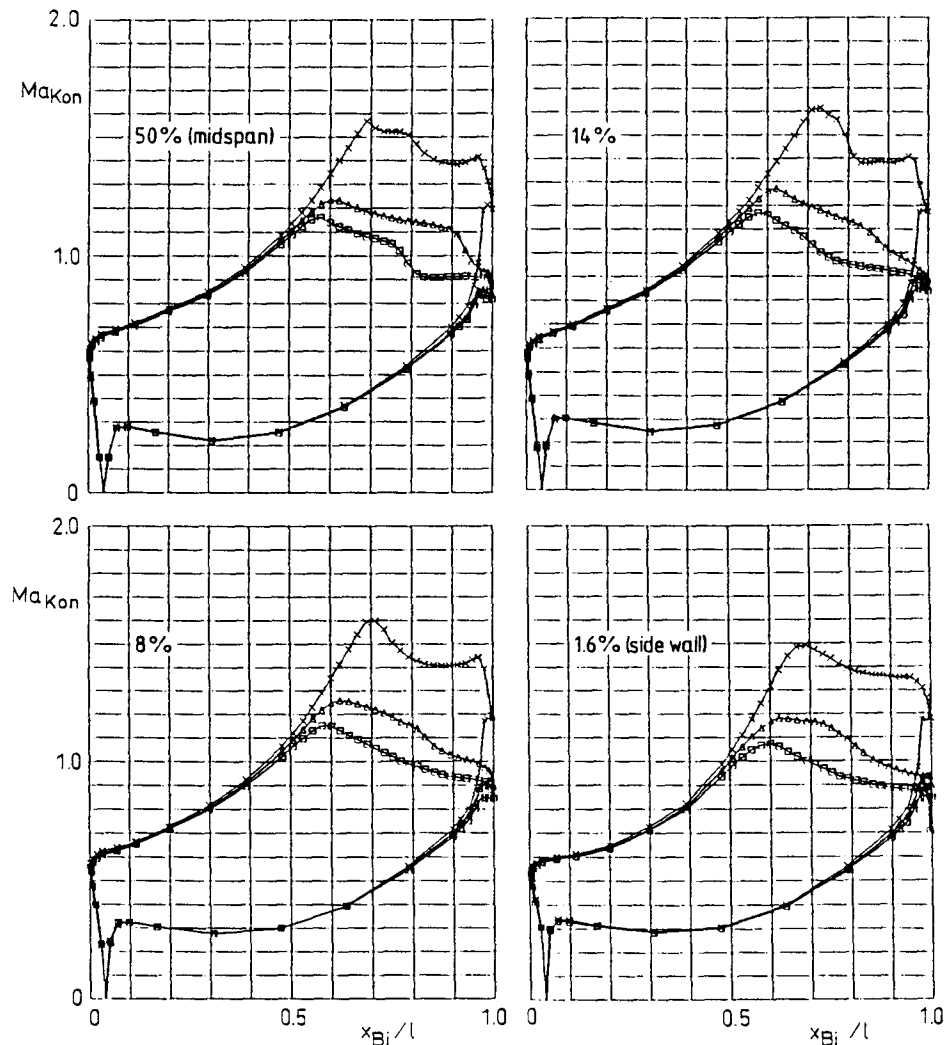

Fig. 8: Profile Mach number distributions for $\beta_1 = 140°$
(X $Ma_2 = 1.25$; $\triangle$ $Ma_2 = 1.0$; $\square$ $Ma_2 = 0.9$)
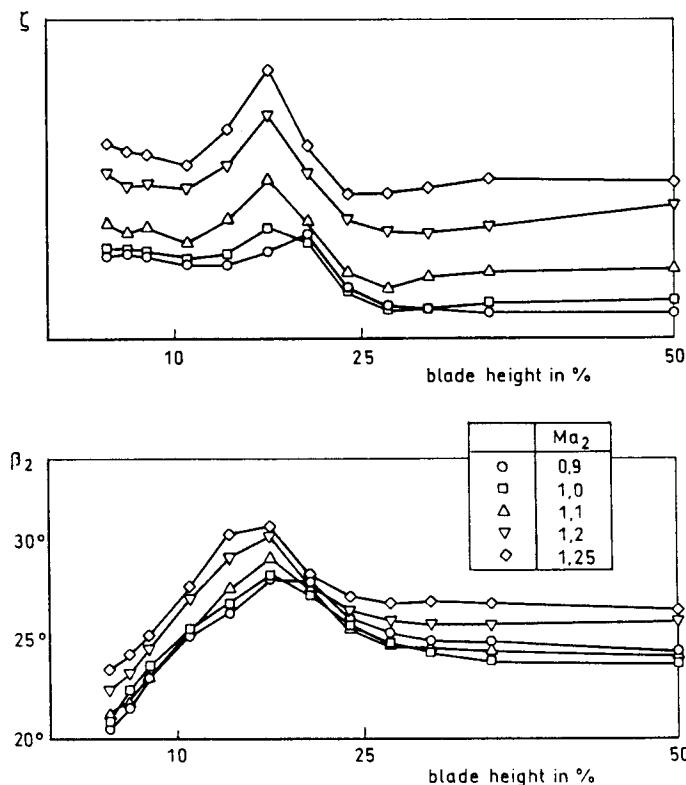
- 6 -

Fig. 11: Comparison of the profile Mach number distribution (X) with the calculation (-) for $\beta_1 = 140°$

Fig. 9: Spanwise total pressure loss ζ distribution (top) and spanwise downstream flow angle β_2 distribution (bottom) for $\beta_1 = 140°$
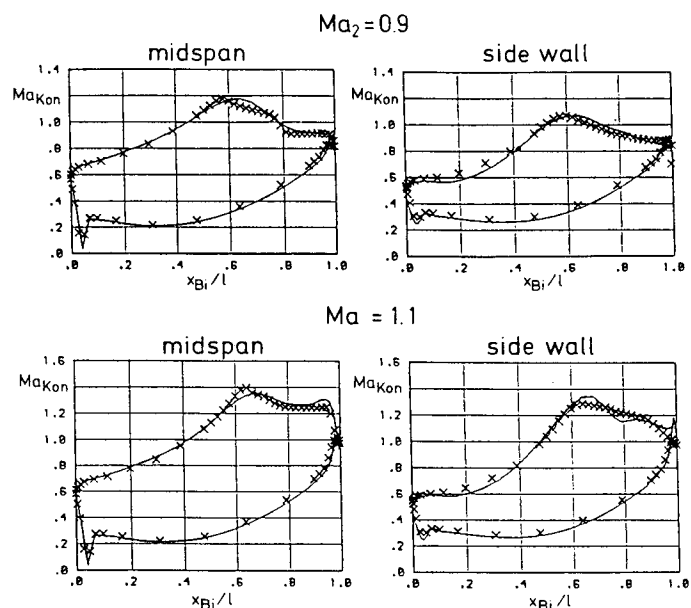

Fig. 10: Comparison of the isobars on the side wall with the calculation for $\beta_1 = 140°$ (increment $\triangle = 0.025$)

gential chord length at midspan disappears at 8 % spanwise blade height due to the influence of the passage vortex. On the side wall at 1.6% spanwise blade height the influence of the passage vortex reduces the profil Mach number in the front part of the suction surface. The velocity decrease at the trailing edge due to the trailing edge shocks occurs for all sections.

Total pressure loss and downstream flow angle are calculated from the results of the wake traverse measurements ([23]). The total pressure loss distributions along the blade span (Fig. 9 top) show strong maxima at the location of the core of the passage vortex. At $Ma_2 = 1.25$ the passage vortex core moved nearer to the side wall. In accordance with the loss distributions the locations of maximum underturning angle (Fig. 9 bottom) also moved nearer to the side wall. These results coincide with the tendency shown by the blade surface oil flow patterns. The corner vortices, however, are not revealed by the wake traverse measurements.

In Figures 10 to 12 the experimental data of the isobars on the side wall, the profile Mach number distributions, the total pressure loss and the downstream flow angle are compared with numerical results. They base on 3D viscous calculations which were carried out for $\beta_1 = 140°$ and $Ma_2 = 0.7, 0.9, 1.1$ ([19], [20]). Figure 10 shows the isobars on the side wall. The data from the experiment and the calculation agree both qualitatively and quantitatively. Figure 11 shows the comparison of the profile Mach number distributions. In the subsonic case, $Ma_2 = 0.9$, at midspan the separation bubble indicated by the plateau as well as the shock indicated by the velocity decrease are not resolved by the calculation. On the side wall the influence of the passage vortex reduces the profile Mach number in the front part of the suction surface. For $Ma_2 = 1.1$ at midspan the impinging upper trailing edge shock bends the profile Mach number distribution. The numerical simulation cannot clearly resolve this interaction. The experimentally observed separation bubbles cannot be obtained numerically. The experimental and numerical results only roughly coincide for the spanwise
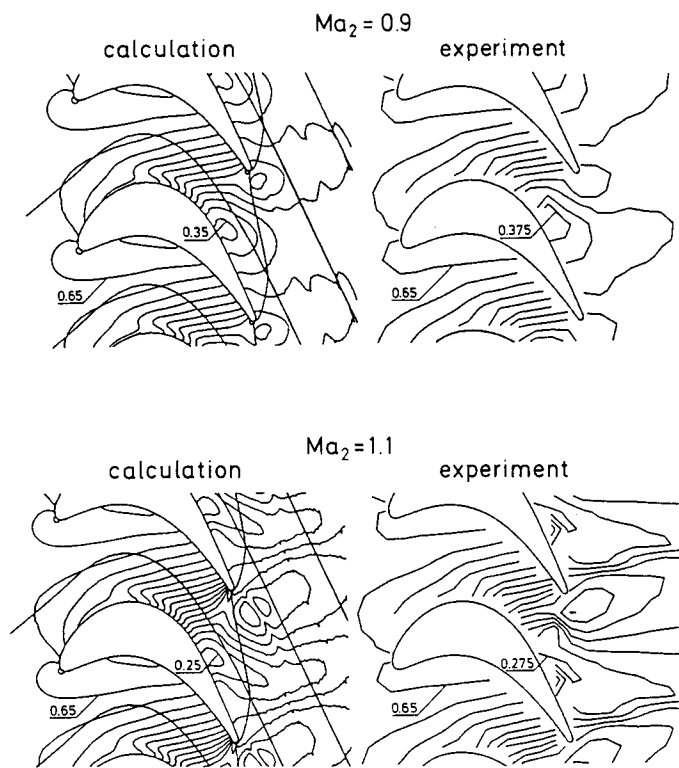
- 7 -

ζ

Ma₂= 0.7

0   25   50

ζ

Ma₂ = 0.9

0   25   50

ζ

Ma₂ = 1.1

—inlet boundary layer

0   25   50

blade height in %

25°

β₂

20°

17°

0   25   50

Ma₂= 0.7

25°

β₂

20°

17°

0   25   50

Ma₂= 0.9

25°

β₂

20°

17°

0   25   50

Ma₂= 1.1

blade height in %

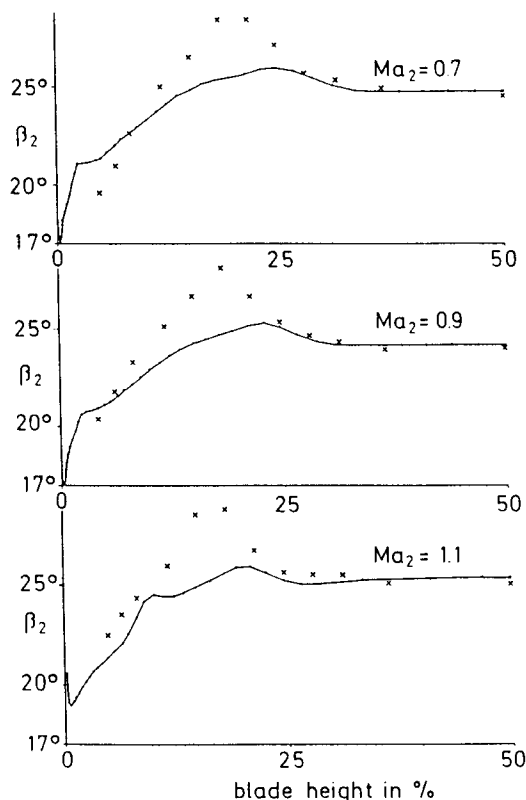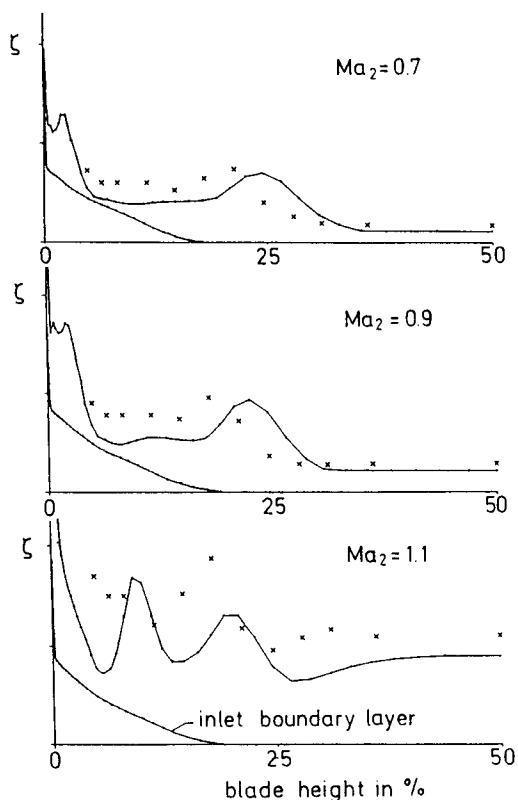Fig. 12: Comparison of the spanwise distributions of the
total pressure loss ζ and downstream flow
angle β₂ (X) with the calculation (-) for β₁ = 140°

total pressure loss distribution and the spanwise down-
stream flow angle distribution (Fig. 12). This discrepancy is
explained in [20] by the used turbulence model.

CONCLUDING REMARKS

The three-dimensional flow field in a transonic turbine
cascade shows shock wave boundary layer interaction and
secondary flow structures depending on the downstream
Mach number and the inlet flow angle. The influence of the
Mach number on the spanwise location of the passage vor-
tex implies the shift of the loss core and the maximum
underturning angle towards the side wall until the cascade
is choked. The influence of the increasing inlet flow angle
results in an extension of the passage vortex towards the
midspan of the blade. The shock wave boundary layer inter-
action does not extend to the side wall region whereas the
trailing edge shocks leave their footprints on the side wall.
The isobars on the side wall and the profile Mach number
distributions at midspan and at the side wall are in good
agreement with the 3D viscous numerical predictions. The
numerical results for spanwise total pressure loss and
spanwise downstream flow angle distributions differ from the
experimental data.

ACKNOWLEDGEMENTS

REFERENCES

[1]   Niehuis, R.; Lücking, P.; Stubert, B.: Experimental and
      Numerical Study on Basic Phenomena of Secondary
      Flows in Turbines. AGARD -CP-469, 1989, pp. 5.1-5.15.

[2]   Sharma, O.P.; Butler, T.L.: Predictions of Endwall
      Losses and Secondary Flows in Axial FLow Turbine
      Cascades. ASME 86-GT-228, 1986.

[3]   Gregory-Smith, D.G.; Graves, C.P.; Walsh, J.A.: Growth
      of Secondary Losses and Vorticity in an Axial Turbine
      Cascade. ASME 87-GT-114, 1987.

[4]   Perdichizzi, A.: Mach number effects on Secondary
      Flow Development Downstream of a Turbine Cascade.
      ASME 89-GT-67, 1989.

[5]   Bassi, F.; Osnaghi, C.; Perdichizzi, A.; Savini, M.: Sec-
      ondary Flows in a Transonic Cascade: Comparison
      between Experimental and Numerical Results. ASME
      J. Fluids Eng. Vol. 111, 1989, pp. 369-377.

[6]   Mee, D.J.; Baines, N.C.; Oldfield, M.L.G.; Dickens, T.E.:
      An Examination of the Contribution to Loss on a Tran-
      sonic Turbine Blade in Cascade. ASME 90-GT-264,
      1990.

[7]   Yamamoto, A.; Nouse, H.: Effects of Incidence on
      Three-Dimensional flows in a Linear Turbine Cascade.
      ASME J. Turbomachinery Vol. 110, 1988, pp. 486-496.

[8]   Hodson, H.P.; Dominy, R.G.: Three-Dimensional Flow
      in a Low-Pressure Turbine Casade at Its Design Con-
      dition. ASME 86-GT-106, 1986.

[9]   Gregory-Smith, D.G.; Cleak, J.G.E.: Secondary Flow
      Measurements in a Turbine Cascade with High Inlet
      Turbulence. ASME 90-GT-20, 1990.

- 8 -

[10] Walsh, J.A.; Gregory-Smith, D.G.: Inlet Skew and the Growth of Secondary Losses and Vorticity in a Turbine Cascade. ASME 89-GT-65, 1989.

[11] Dietrichs, H.-J.; Hourmouziadis, J.; Malzacher, F.; Bräunling, W.: Flow Phenomena in Transonic Turbine Cascades. Detailed Experimental and Numerical Investigation. Proc. 8th ISABE, Cincinnati, Ohio, USA, 1987.

[12] Bräunling, W.; Quast, A.; Dietrichs, H.-J.: Detection of Separation Bubbles by Infrared Images in Transonic Turbine Cascades. ASME 88-GT-33, 1988.

[13] Kost, F.; Bräunling, W.; Schüpferling, E.; Göhl, R.: Detection of Separation Bubbles by Heated Thin-Film Sensors in Transonic Turbine Cascades. Proc. 9th Symp. on Measuring Techniques for Transonic and Supersonic Flows in Cascades and Turbomachines, Oxford, U.K., 1988.

[14] Langston, L.S.; Nice, M.L.; Hooper, R.M.: Three-Dimensional Flow Within a Turbine Cascade Passage. ASME J. Eng. Power Vol. 99, 1977, pp. 21-28.

[15] Marchal, Ph.; Sieverding, C.H.: Secondary Flows within Turbomachinery Bladings. Secondary Flows in Turbomachines, AGARD-CP-214, 1977.

[16] Sieverding, C.H.: Recent Progress in the Understanding of Basic Aspects of Secondary Flows in Turbine Blade Passages. ASME 84-GT-78, 1984.

[17] Stanewsky, E.: Shock Boundary Layer Interaction in Transonic and Supersonic Flow. Transonic Flows in Turbomachinery, VKI Lecture Series 59, Rhode Saint Genes, Belgium, 1973.

[18] Delery, J.; Marvin, J.G.: Shock-Wave Boundary Layer Interactions. AGARD-AG-280, 1986.

[19] Zimmermann, H.: Calculation of Two- and Three-Dimensional Flow in a Transonic Turbine Cascade with Particular Regards to the Losses. AIAA 21st Fluid Dynamics, Plasmaphysics and Laser Conference, June 18-20, 1990, Seattle. AIAA 90-1542, 1990.

[20] Zimmermann, H.: Berechnung von zwei- und dreidimensionalen Strömungen in einem transsonischen Trubinengitter unter besonderer Berücksichtigung der Verluste. Ph.D.Thesis, ZLR-Forschungsbericht 90-03, Braunschweig, 1990.

[21] Heinemann, H.-J.: The Test Facility for Rectilinear Cascades (EGG) of the DFVLR. DFVLR-IB 222 - 83 A 14, 1983.

[22] Lawaczeck, O.; Amecke, J.: Aufbau und Eichung einer neuentwickelten Keilsonde für ebene Nachlaufmessungen, insbesondere im transsonischen Geschwindigkeitsbereich. DLR FB 70-69, 1970.

[23] Amecke, J.: Data Reduction of Wake Flow Measurements with Plane Cascades. DLR IB 222 - 90 A 06, 1990.

[24] Detemple-Laake, E.: Measurement of the Flow Field in the Blade Passage and Side Wall Region of a Plane Turbine Cascade. AGARD-CP-469, 1989, pp.10.1.-10.12.